LAWRENCE
LIVERMORE
NATIONAL
LABORATORY

LLNL-JRNL-827499

Effect of substrate temperature on sputter-deposited boron carbide films

L. B. Bayu Aji, S. J. Shin, J. H. Bae, A. M. Engwall, J. A. Hammons, X. Lepro Chavez, N. Catarineu, P. B. Mirkarimi, S. O. Kucheyev

October 4, 2021

Journal of Applied Physics

Disclaimer

Effect of substrate temperature on sputter-deposited boron carbide films

L. B. Bayu Aji,[1] S. J. Shin,[1] J. H. Bae,[2] A. M. Engwall,[1] J. A. Hammons,[1]
X. Lepro Chavez,[1] N. Catarineu,[1] P. B. Mirkarimi,[1] and S. O. Kucheyev[1]

[1] *Lawrence Livermore National Laboratory, Livermore, California 94550, U.S.A.*
[2] *General Atomics, San Diego, California 92186, U.S.A.*

(Dated: October 8, 2021)

Sputter deposition of B_4C films with tailored physical properties remains a challenge. Here, we systematically study how substrate temperature influences properties of B_4C films deposited by direct current magnetron sputtering onto planar substrates held at temperatures in the range of 100−510 °C. Results show that all films are amorphous stoichiometric B_4C, with O content of ~ 1 at.%. Films deposited onto substrates at 100 °C exhibit high compressive residual stress and decreased mechanical properties. For elevated substrate temperatures in the range of $180 - 510$ °C, film mass density, surface roughness, Young's modulus, and hardness are weakly dependent on substrate temperature. However, in this temperature range, an increase in substrate temperature leads to larger residual compressive stress, accompanied by a corresponding reduction in the concentration of nanoscale inhomogeneities. The overall weak substrate temperature dependence of film properties revealed in this work is favorable for the development of a robust deposition process, particularly for the case of deposition onto non-planar substrates where temperature control is often challenging.

I. INTRODUCTION

Boron carbide (B_4C) is a unique material with an outstanding combination of low mass density, high chemical resistance, excellent tribo-mechanical properties, and large neutron absorption cross-sections.[1] As a result, B_4C films are attractive for several applications, including a wide range of tribological coatings,[1–5] x-ray optics,[6–8] neutron detectors,[9,10] the plasma-facing first wall in magneto-fusion reactors,[11] chemically-resistant components in semiconductor processing tools,[12] and hydrogen fuel ablator capsules for inertial confinement fusion (ICF).[13–18] This latter, ICF-related application, which is the driving force of the present study, calls for ultrathick B_4C films ($\gtrsim 10$ μm) with uniform density at length scales of $\gtrsim 100$ nm. Growth of such thick films is typically limited by residual stresses causing undesirable delamination, deformation, and/or fracture.

A number of previous reports have demonstrated the fabrication of B_4C films by direct current magnetron sputtering (DCMS).[2–4,6–10,14,17–24] These reports have clearly identified large residual compressive stress, typically exceeding 1 GPa, as the main challenge limiting applications of B_4C. Recently,[17] we have systematically studied the Ar working gas pressure dependence, revealing a deposition parameter space resulting in smooth, high-purity, amorphous B_4C films with near-zero total residual stress. As a result, the deposition of ~ 10-μm-thick B_4C films has been demonstrated.[17] These favorable deposition conditions of films with low residual stress involve the substrate holder held at 450 °C and a relatively high Ar working gas pressure range of $18 - 22$ mTorr with a target-to-substrate distance (TSD) of 50 mm, leading to low energetics and a broad angular distribution of landing atoms.[17] However, despite having low residual stress, resultant films have featured reduced densities and mechanical properties compared to those for films made at lower Ar gas pressures.[17] Hence, further studies are required to explore the process parameter space and to better understand the physics of B_4C film growth.

In addition to working gas pressure and the TSD, which determine the ballistics of depositing species flux, substrate temperature (T_s) is another major process parameter that controls film growth and, therefore, film properties.[25–28] Substrate temperature determines thermally-activated diffusional and reaction processes of adatoms and point defects that influence intrinsic stress in films, adsorption and desorption of residual gas molecules and their byproducts, the evolution of the system toward thermodynamic equilibrium, and the thermal component of residual stresses in films.

The effect of T_s on properties of sputter deposited B_4C films has been reported for both DCMS[3,9,21,22] and radio-frequency magnetron sputtering (RFMS)[29–34] cases albeit with inconsistent results of the effect of T_s on film stoichiometry, density, residual stress, and mechanical properties. In some cases, this discrepancy, described in more detail below, could be related to the uncertainty in actual T_s values since the temperature typically reported is the temperature of the substrate holder (T_{holder}) rather than T_s. As we demonstrate below, the difference between T_s and T_{holder} could be appreciable for the case of B_4C deposition, particularly at elevated temperatures when radiative heat transport dominates because the B_4C surface has high emissivity.[35]

Here, we systematically study B_4C films deposited under Ar pressure and TSD conditions identified in our recent study,[17] reporting a close-to-zero residual stress state, with T_s varied in the range of $100 - 510$ °C (corresponding to the T_{holder} range of $20 - 700$ °C). Our results confirm previously reported challenges of high residual stress for B_4C films deposited at T_s values close to room temperature.[6–8,10,19,20,23] They also reveal that all the key film properties, including density, microstructure, residual stress, and mechanical properties are only

TABLE I. Conditions used to deposit B_4C films in the present study by DCMS with a 76-mm-diameter magnetron source. The gas flow rate is given in standard cubic centimeters per minute (sccm).

Power	300 W
Target-to-substrate distance	5 cm
Ar pressure	18 mTorr
Ar gas flow	25 sccm
Ar purity	99.998%
Substrate temperature	$100 - 510$ °C
Film thickness	$0.9 - 1.3$ μm
Deposition time	$100 - 120$ min
Deposition rate	$0.45 - 0.55$ μm/hour
Target voltage	$435 - 538$ V
Target current	$583 - 701$ mA

weakly dependent on T_s in a wide range of moderately elevated temperatures from 180 to 510 °C.

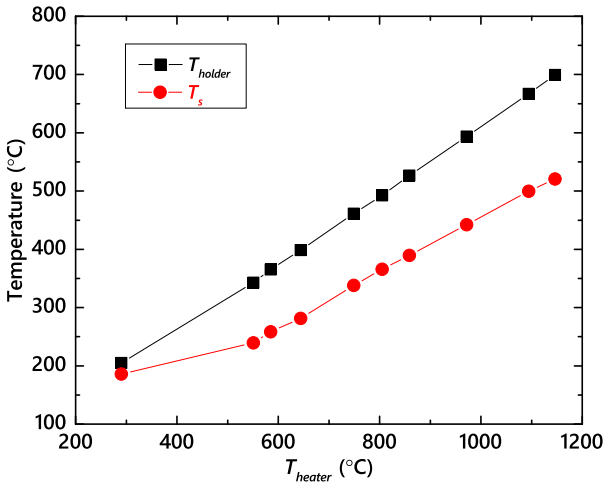

FIG. 1. Relationship between temperatures of the heater (T_{heater}), the substrate holder (T_{holder}), and substrates (T_s). Error bars of the temperature measurement are ± 5 °C.

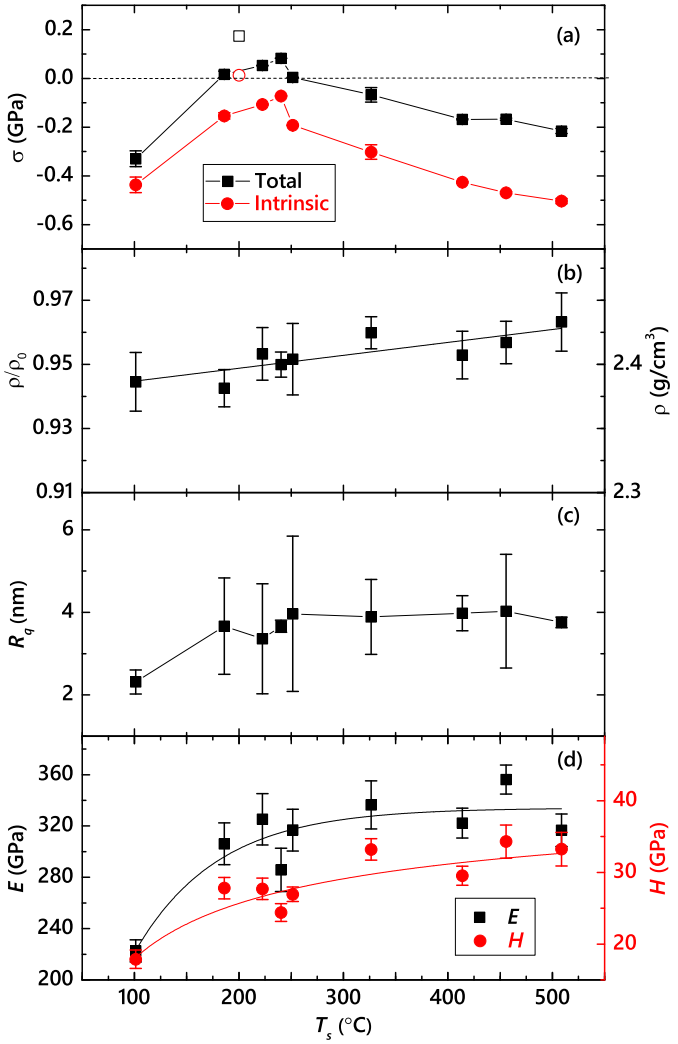

FIG. 2. Substrate temperature dependencies of (a) total and intrinsic (with the thermal stress component subtracted) residual stress (σ), (b) mass density (ρ, where $\rho_o = 2.52$ g/cm^3 is the theoretical maximum density of crystalline B_4C), (c) surface roughness (R_q) measured over an area of $\sim 20 \times 20$ μm^2, (d) Young's modulus (E), and Meyer's hardness (H). Open symbols in (c) are for a 16-μm-thick film. Solid lines through data points in (b) and (d) are to guide the reader's eye.

II. EXPERIMENT

A. Sputter deposition

Films were made by DCMS in a cylindrical high-vacuum chamber with a diameter of 44 cm and a height of 36 cm and a base pressure of $\sim 5 \times 10^{-7}$ Torr, with the substrate and chamber walls kept at $\sim$ 30 °C. The chamber was equipped with a 76-mm-diameter planar magnetron gun (MAK model from MeiVac Inc.). The B_4C deposition target was 63.5 mm in diameter with an initial thickness of 9.3 mm, bonded to a 76-mm-diameter, 3.2-mm-thick Cu backing plate. All depositions were performed in the so-called sputter-down configuration in a constant power mode under conditions summarized in Table I. Slight variations in target voltage and current and the deposition rate between different runs were due to target wear (erosion) during the course of these experiments.

Several types of substrates were used, including 50-mm-diameter Si (100) and c-plane Al_2O_3 wafers, 10×10 mm^2 Si (100) chips, and 12×12 mm^2 polycrystalline Cu coupons. Prior to deposition, all substrates were cleaned with ethanol followed by an exposure of Si and sapphire substrates to air plasma to remove residual carbon contaminants. Substrates were positioned under the magnetron target on an electrically grounded disk-shaped Mo holder, with a diameter and thickness of 89 and 4 mm, respectively. This Mo holder was rested on a 76-mm-

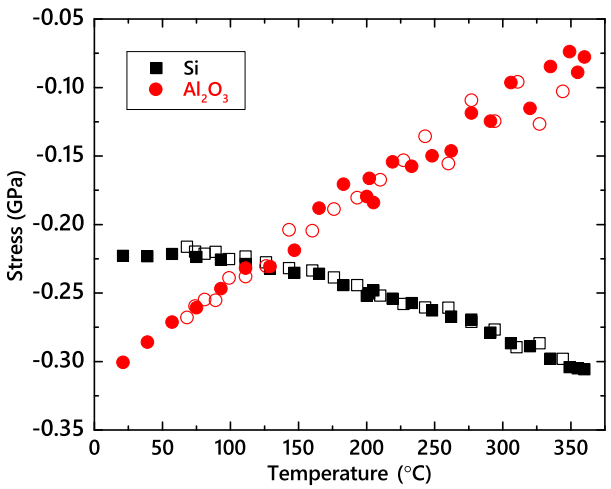

FIG. 3. Residual stress of B_4C films on Si (100) and *c*-plane Al_2O_3 substrates as a function of temperature during CTE measurements performed after film deposition. Heating and cooling curves are shown by closed and open symbols, respectively.

diameter Mo-body resistive heater (model 102193 from HeatWave Labs Inc.).

B. Thermometry

Temperatures of the heater (T_{heater}), the disk-shaped substrate holder (T_{holder}), and substrates (T_s) were monitored separately. Thermocouples (K-type) were used to measure T_{heater} and T_{holder}, while T_s was measured by imaging pyrometry (model PI 640 from Optris GmbH) through a ZnSe port. Values of effective emissivity and transmissivity were obtained from calibration runs involving imaging a B_4C coated Mo substrate holder whose temperature was monitored with thermocouples. Figure 1 shows the relationship between T_{heater}, T_{holder}, and T_s, illustrating that the difference between T_{holder} and T_s increases at higher temperatures. In order to reach higher T_s values with the resistive heater rated up to 1200 °C, a better thermal coupling between the holder and heater was required. Hence, both top and bottom surfaces of the Mo disk holder and the top surface of the Mo-body heater were pre-coated with B_4C to increase their emissivity. Note that, in our recent work,[17] the quoted temperature of 450 °C referred to T_{holder} (measured with thermocouples in both studies) rather than to T_s (measured by imaging pyrometry in the present study). With the aid of this additional pyrometry, we can estimate that this corresponds to a T_s of $\sim$ 330 °C in our previous study.[17]

The low limit of T_s (100 °C) in the data set presented here was determined by native plasma heating. With no additional substrate heating, T_s sharply increased from 30 to 95 °C in the first 10 min of the deposition run. The

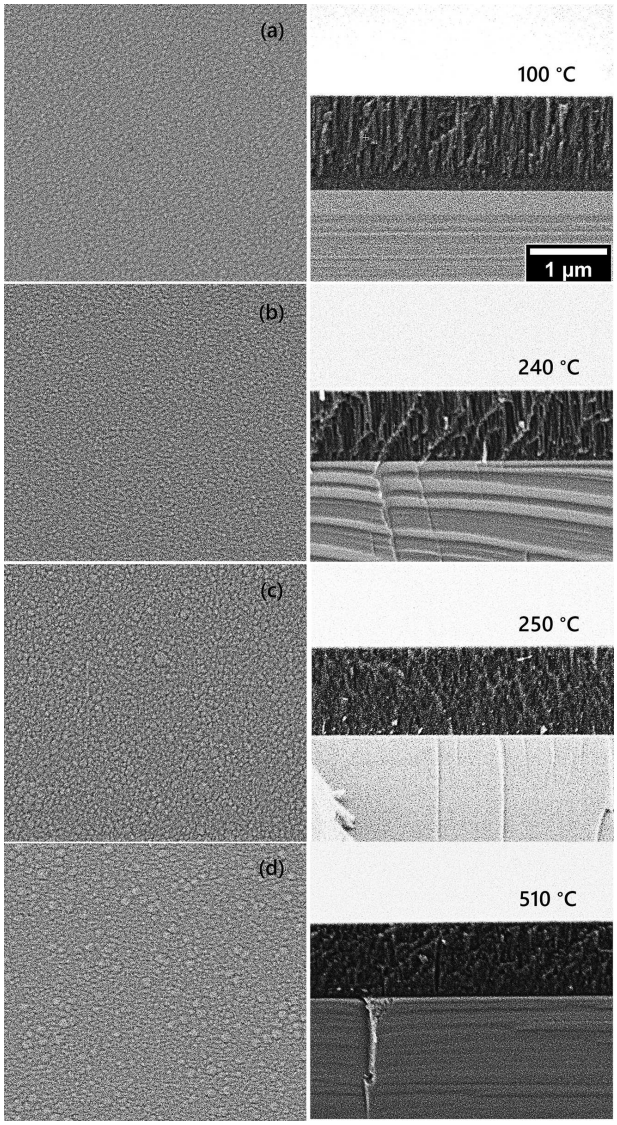

FIG. 4. (Left column) plan-view and (right column) cross-sectional SEM micrographs of B_4C films deposited at substrate temperatures of (a) 100, (b) 240, (c) 250, and (d) 510 °C. All panels are of the same magnification.

T_s increased from 95 to 105 °C for the remaining 90 min of the deposition run.

C. Film characterization

Rutherford backscattering spectrometry (RBS) was employed to measure the compositional depth profile in all the films. Samples were bombarded with a 2 MeV $^4He^+$ ion beam incident normal to the film surface and scattered into a detector at 165° from the incident beam direction. The analysis of RBS spectra was performed with the RUMP code.[36] Measurements of areal density, possible in this scattering geometry for films with thicknesses of $\lesssim$ 1.3 μm, were performed based on the fact

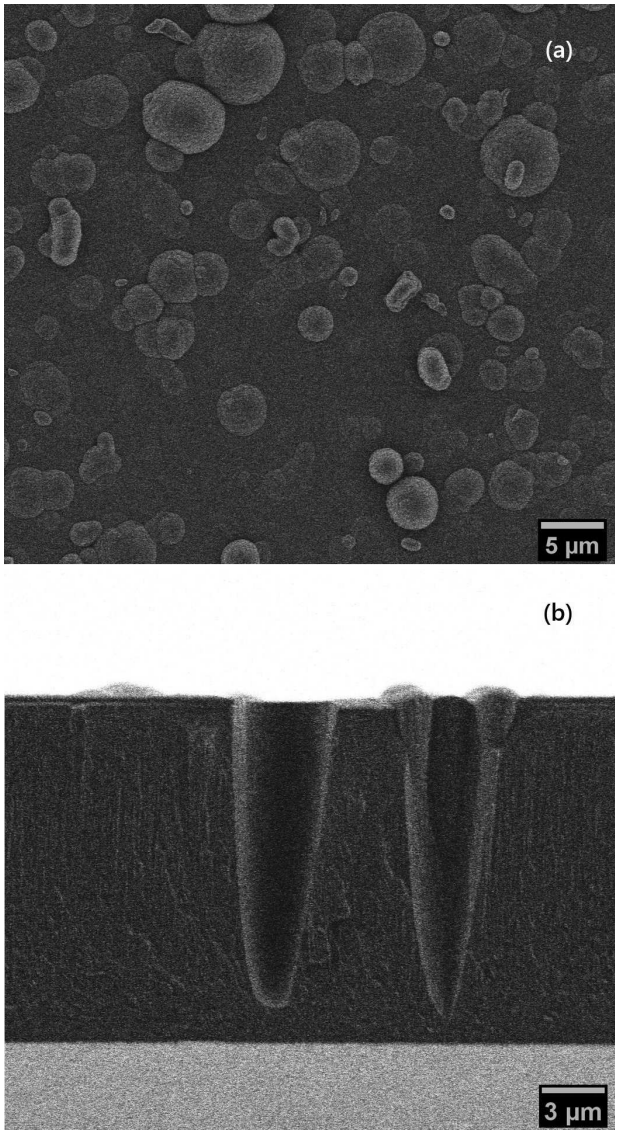

FIG. 5. (a) Plan-view and (b) cross-sectional SEM micrographs of a 16-μm-thick B_4C film deposited at a substrate temperature of 200 °C.

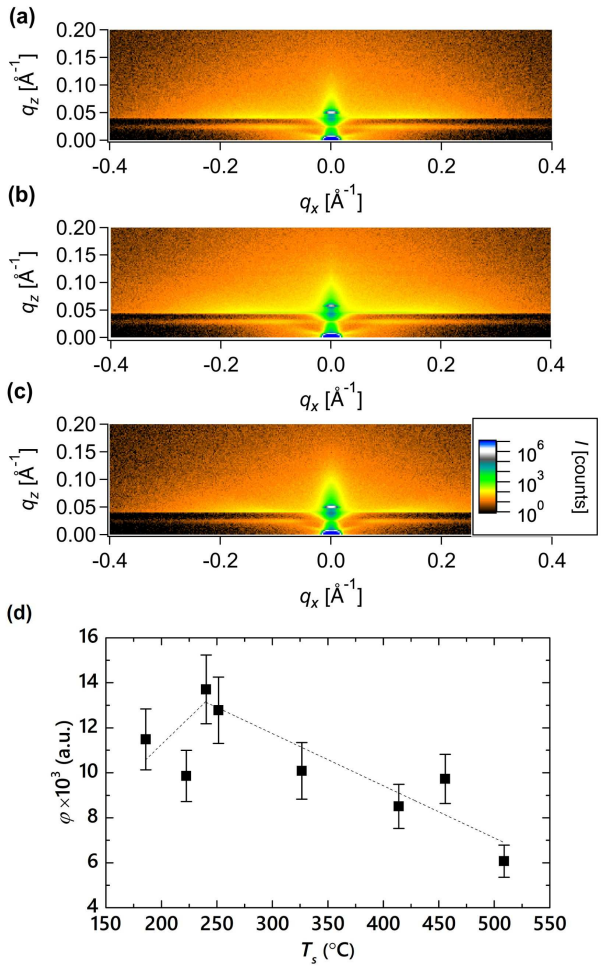

FIG. 6. GISAXS results for B_4C films deposited at substrate temperatures of (a) 185, (b) 240, (c) 510 °C. The intensity scale in (c) refers to panels (a)–(c). (d) Substrate temperature dependence of the GISAXS-derived scattering scaling factor (φ), which is a measure of the degree of density heterogeneity in films.

that the probing He ion beam experienced energy loss while passing through the B_4C layer. Areal density is, therefore, proportional to the energy shift of the scattering signal from the Si substrate.

Physical thickness of films was first measured by conventional stylus profilometry (model D-100 from KLA-Tencor). More accurate thickness measurements, required for mass density analysis, were done by cross-sectional scanning electron microscopy (SEM) in a Thermofisher Apreo instrument operating at 2 kV. For all films, cross-sections were prepared by mechanical fracture at room temperature. Mass density was calculated by dividing the areal density measured with RBS by the physical thickness measured by SEM. A Keyence VK-X1000 laser confocal microscope was used for root mean square surface roughness (R_q) measurements over an area of $\sim 20 \times 20$ μm^2. The crystallographic structure of films was probed by X-ray diffraction (XRD) with a Bruker-AXS Discover D8 diffractometer equipped with a Cu K-α source.

A Tohu Technology FLX-2320-S tool was used to measure average residual stress (σ) of all the films deposited on 50-mm-diameter wafers. This system uses lasers of two different visible wavelengths to measure the curvature (κ) of the substrate prior to and after film deposition. The measured κ was related to σ by the Stoney equation:[37,38]

$$\kappa = \frac{6\sigma h_f}{M_s h_s^2}, \tag{1}$$

where h_f and h_s are thicknesses of the film and substrate, respectively, and M_s is the biaxial modulus of the substrate. In these calculations, we used a M_s of 180.3 GPa

for Si taken from the literature.[37] The Stoney equation relies on the assumption that the deposited film itself has a negligible contribution to the bending resistance, which is a reasonable approximation for this case when film thickness (~ 1 μm) is insignificant compared to that of the substrate (280 μm).

Since B_4C deposition involves elevated T_s, residual stress contains a contribution originating due to the difference in coefficients of thermal expansion (CTE) of the film and substrate. Because we are not aware of any previous reports of CTE values for amorphous B_4C films, we have performed such measurements. For two films deposited on Si and *c*-plane Al_2O_3 wafers, σ was measured as a function of temperature (T), and the CTE was estimated based on the following equation:

$$\frac{d\sigma}{dT} = M_f(\alpha_f - \alpha_s), \tag{2}$$

where $M_f = \frac{E_f}{(1-\nu_f)}$ is the biaxial modulus of the film; α_s and α_f are CTEs of the substrate and film, respectively; and E_f and ν_f are the Young's modulus and Poisson's ratio of the film, respectively. Two temperature cycles were performed with each substrate. We used the second temperature cycles to reduce the potential impact of intrinsic stress relaxation on the measurements.

Mechanical properties were evaluated by indentation in the load-controlled mode with an MTS XP nanoindenter with a Berkovich diamond tip. Meyer's hardness (H) was defined as average contact pressure, and Young's modulus of the film (E_f) was calculated based on the Oliver-Pharr method.[39] In Oliver-Pharr calculations, we assumed Poisson's ratios of diamond and B_4C films of 0.07 and 0.17, respectively, and a Young's modulus of diamond of 1141 GPa.[1,40] Values of H and E_f were averaged over the indenter penetration depth range of $\sim 10-20\%$ of film thickness.

The refractive index of the films was measured by spectroscopic ellipsometry (model M-2000 from J.A. Woollam Co.) at several different locations on each sample with an incident beam diameter and angle of 125 μm and 70°, respectively. Optical constants were obtained by fitting the amplitude (Ψ) and phase difference (Δ) components to a mathematical spline model under Kramers-Kroning conditions to ensure physical consistency.

Grazing-incidence small-angle X-ray scattering (GISAXS) was employed to resolve nanoscale heterogeneity of electron density within films. A Xeuss 3.0 instrument with an X-ray beam from a Cu-α source was used. Samples were positioned on the holder in such a way that the film surface was close to parallel to the X-ray beam propagation direction (y-direction), with the film surface defining the xy plane and the surface normal in the z-direction. An X-ray beam size of 1.0×0.5 mm^2 illuminated the samples at glancing tilt angles of $0.0-0.2°$ between the beam and the film plane. A Pilatus3 300k detector was used in "line-erasure" mode whereby two images were obtained to remove the dead zones on the detector. The sample to detector distance was calibrated with silver behenate. The 2D images were analyzed with FitGISAXS module for Igor Pro[41] and shown in reciprocal space units (q_x, q_y, q_z). Here, q_x and q_y are parallel to the X-ray beam, and q_z is perpendicular to it. More details of the GISAXS modeling and fitting analysis can be found in the supporting information.

III. RESULTS AND DISCUSSION

1. Crystallography

The deposited films are amorphous for the entire T_s range studied here ($100-510$ °C), as indicated by the absence of B_4C related Bragg peaks in XRD scans (not shown). This observation is in agreement with negligible changes to the short range order and bonding, studied by electron diffraction and infrared spectroscopy, respectively, reported by Bao and Chrisey[29] for thin films deposited by RFMS at T_{holder} in the range of $20-650$ °C. It is also consistent with previous reports[21,30] that T_{holder} above $\sim$ 900 °C is needed to grow crystalline B_4C by sputter deposition from B_4C targets as T_{holder} was limited to $\sim$ 700 °C in the present study (Fig. 1). Since the correlation between T_s and T_{holder} depends on the details of the specific experimental setup and substrate properties, it is possible that the growth of crystalline B_4C could be observed at T_{holder} lower or higher than 900 °C. Future studies with better controlled T_s are needed to clarify how the transition between growth modes of amorphous and crystalline B_4C depends on T_s as well as on landing particle ballistics and the growth rate.

2. Elemental composition

The ratio of B to C atomic concentrations, the presence of impurities, and the areal density of films were measured with RBS. For all values of T_s studied, films were stoichiometric B_4C, reflecting the stoichiometry of the sputter target (also analyzed by RBS), with ~ 1 at.% of O, and Ar content below the detection limit of these RBS measurements ($\lesssim 0.2$ at.%). Such a low concentration of Ar is expected from the favorable ballistics and the low plasma potential typical for DCMS plasmas ($\lesssim 5$ eV).[42] Low O content is in agreement with results of our previous study with a T_{holder} of 450 °C.[17]

The observation that the B/C stoichiometric ratio is independent of T_s is in agreement with the report by Kulikovsky et al.,[21] who studied the T_{holder}-dependence of B_4C film properties deposited by DCMS at a T_{holder} of $\lesssim 970$ °C with a 75-mm-diameter target run at 300 W, with a TSD of 50 mm, an Ar pressure of 4 mTorr, and a grounded substrate holder. In contrast, Han et al.[31] have reported that the B/C atomic ratio of B_4C films deposited by RFMS decreases with increasing T_{holder} and

reaches $\sim$ 3 for a T_{holder} of 450 °C. It is not clear if this stoichiometric imbalance is related to peculiarities of RF plasma excitation and gas phase transport of atoms between the target and the substrate or limitations of compositional analysis. Further work is currently needed to better understand effects of plasma parameters on the stoichiometry of B_4C films.

A remarkable observation of the present study is that O content in films ($\sim$ 1 at.%) is below that in the starting B_4C target ($\sim$ 2.5 at.%) and is independent of T_s despite the fact that the base pressure of the chamber (and, hence, the partial pressure of water during deposition) with the heater turned on was varying in a wide range of $(5-200)\times10^{-7}$ Torr in these experiments. The base pressure was higher for larger T_{heater}. These observations suggest that the growing B_4C film is not efficient at gettering O-containing species in vacuum, likely due to volatility of resultant O-containing molecules as suggested previously.[17] This observation of low O content being insensitive to the chamber base pressure is favorable for the development of a robust and economical process of the deposition of high-purity B_4C films without resorting to more demanding ultra-high vacuum conditions.

3. Residual stress

The evolution of total residual stress in films deposited at different T_s is shown in Fig. 2(a). It is seen that films deposited at the lowest T_s studied (100 °C) are under compressive stress of 0.33 GPa. This is consistent with numerous previous observations (including our own unpublished results for deposition with a 33-mm-diameter sputter source) of residual-stress-related challenges with the deposition of thick B_4C films on unheated substrates. For the T_s range of $185-250$ °C, films are under slight tensile total residual stress. The total residual stress changes again from tensile to compressive for $T_s \gtrsim 250$ °C.

Also plotted in Fig. 2(a) is intrinsic residual stress, which is the total stress without the thermal stress component originating from the difference in the CTE of the film and the substrate. Such a thermal stress component is important to consider for deposition onto substrates at elevated temperatures. The thermal stress component was calculated with Eq. 2 with a usual assumption that M_f, α_f, and α_s are temperature independent. In the calculations, we used the following parameters: T_s measured by pyrometry, $\nu_f = 0.17$,[1] $\alpha_s = 3.63\times10^{-6}$ K^{-1},[43] E_f measured by indentation [Fig. 2(d)], and $\alpha_f = (4.7\pm0.3)\times10^{-6}$ K^{-1} calculated based on measurements of the evolution of σ as a function of temperature for two films deposited on Si and *c*-plane Al_2O_3 wafers (Fig. 3). This CTE value for amorphous B_4C films is comparable to an average value of 5.7×10^{-6} K^{-1} reported for bulk polycrystalline B_4C ceramics in a very wide temperature range of 20–2240 °C.[1,44]

Since the CTE of B_4C is larger than that of the Si substrate, the thermal stress component is tensile, increasing linearly from 0.1 to 0.3 GPa with increasing T_s from 100 to 510 °C, according to Eq. 2. Figure 2(a) shows that, with the thermal component subtracted, intrinsic residual stress is compressive and relatively low ($|\sigma| \lesssim 0.5$ GPa) in the entire T_s range studied, and the dependence of intrinsic residual stress on T_s remains non-monotonic. Based on these results, the favorable T_s range resulting in low intrinsic residual stress is between 185 and 250 °C. We then deposited a 16-μm-thick film on a Si substrate at T_s of 200 °C. This thick film had a total residual stress of $\sim$ 0.2 GPa (tensile) with near-zero intrinsic residual stress [open symbols in Fig. 2(a)]. Such a reduction in the intrinsic residual stress for the 16-μm-thick film indicates a (weak) dependence of residual stress on film thickness and could be attributed to the evolution of film microstructure.

The total residual stress could be controlled with thremal stress by the choice of the substrate with a CTE resulting in the desired total stress. For most applications, small compressive stress ($|\sigma| \sim 0.1-0.3$ GPa) is desired given lower mechanical strength of most brittle materials (such as B_4C) under tension compared to compression. This calls for substrates with the CTE close to that of B_4C, such as Ti, Cr, Ge, GeO_2, or Ta.[45]

Jacobsohn et al.[23] has considered effects of Ar impurities in the explanation of residual stress behavior of B_4C films. Such impurity effects, also often invoked to explain residual stress evolution in metallic films,[46] could be ruled out for the B_4C films reported here as their composition is independent of T_s, as discussed in Sec. III 2. The main effect of T_s on film growth is an increase in the rate of thermally activated diffusional processes including adatoms and subsurface point defects. The non-monotonic behavior of stress revealed by Fig. 2(a) could be attributed to a combination of the evolution of film homogeneities, described below, and the kinetics of the clustering and annihilation of point defects, particularly at higher T_s values.

The general trend of an increase in intrinsic compressive stress with increasing T_s is in qualitative agreement with observations by Pascual et al.,[32] who reported a slight increase in compressive stress from 4.5 to 5.5 GPa with increasing T_{holder} from 300 to 500 °C in a study of $(0.5-1.1)$-μm-thick B_4C films deposited by RFMS. However, such a comparison with the present work has limitations because of the RF plasma excitation and very high intrinsic compressive stress values of $\sim$ 5 GPa in the work by Pascual et al.[32] indicate a very different deposition regime from the close-to-zero total stress regime investigated here. The importance of other deposition parameters on stress behavior can be illustrated by a comparison with results of a more recent report by Schmidt et al.,[22] who studied $\lesssim$ 2-μm-thick B_4C films deposited by DCMS with a large square target with an area of 210×210 mm^2 powered at 3.5 kW with the Ar gas pressure varied in the range of $2-6$ mTorr (with the TSD value not specified)

and T_{holder} of 100 and 400 °C. That study[22] reported a reduction in total compressive stress from ~ 0.3 to ~ 0.2 GPa on increasing T_{holder} from 100 to 400 °C at 2 mTorr. However, at 4.5 and 6 mTorr, T_s effect on total residual stress was negligible. These observations call for further studies to better understand the effect of the deposition parameters on residual stress of B_4C films.

4. Density

The T_s dependence of film mass density (ρ) is summarized in Fig. 2(b), showing that ρ values are similar for all the films studied, exhibiting only a slight and monotonic increase from 2.41 to 2.43 g/cm^3 with increasing T_s. This corresponds to the range of $\sim 94.7 - 95.5$ % of the full density crystalline B_4C with 2.52 g/cm^3.[45] Importantly, a comparison of Figs. 2(b) and 2(a) reveals lack of correlation between T_s dependencies of film density and residual stress, indicating that these two properties can be controlled independently in this range.

5. Microstructure and surface morphology

Figure 4 shows a collage of (left column) plan-view and (right column) fracture-prepared cross-sectional SEM micrographs for films deposited at T_s between 100 and 510 °C. For all T_s values, plan-view micrographs show smooth surfaces. The T_s dependence of surface roughness (R_q) is plotted in Fig. 2(c), showing that R_q is in the range of $2 - 4$ nm and, within the error bars of these measurements, is independent of T_s. This is in agreement with qualitative observations based on plan-view SEM micrographs from Fig. 4.

Cross-sectional micrographs in the right column of Fig. 4 reveal a columnar structure for films deposited at 240 °C and below [Figs. 4(a) and 4(b)] and no evidence of the columnar structure for films deposited at 250 °C and above [Figs. 4(c) and 4(d)]. A comparison of Figs. 4 and data from our previous studies[17,18] of films deposited at a T_s of 330 °C reveals that, at least at this T_s, such loss of the columnar structure (visualized in SEM micrographs from fracture-prepared cross-sections) is observed only in the first ~ 3 μm of the film, while thicker films exhibit a columnar microstructure.

The columnar structure in vapor deposited films is commonly observed only in a certain T_s range, which can be attributed to an interplay between ballistic atomic shadowing and adatom diffusion.[26,47–50] Hence, loss of the columnar structure with increasing T_s above 240 °C observed in Figs. 4 is in agreement with an expected increase in adatom mobility at higher temperatures. Mechanisms of such a mobility increase are, however, not clear. Indeed, a T_s of 240 °C corresponds to only 17% of the melting point of the B_4C (3036 K),[45] which is even lower than homologous temperatures of $\sim$ 30% (i.e., $\sim$ 638 °C for B_4C) commonly required for the onset of the formation of a columnar structure (sometimes referred to as "zone I") and much lower than homologous temperatures of $\gtrsim 50\%$ ($\gtrsim 1245$ °C for B_4C) when bulk diffusion is expected to become active (zone II), resulting in loss of the columnar structure. Alternatively, such temperature effects on film morphology could be related to the desorption of residual gas impurities (water and its byproducts in the present study) on adatom mobilities. Additional studies are currently needed to better understand these phenomena.

Figure 5 shows plan-view and cross-sectional SEM micrographs of a 16-μm-thick B_4C film deposited at a T_s 200 °C. The film exhibits a uniform columnar structure throughout film thickness. Also clearly seen in both plan-view and cross-sections in Fig. 5 are so called nodular defects that have domed tops [Fig. 5(a)] and close-to-parabolic walls [Fig. 5(b)]. The nodule diameter varies from 0.5 to 5 μm, suggesting that they seed continuously during film growth. Such nodular defects have been observed in all previous studies of DCMS-deposited B_4C films with thicknesses above $\sim$ 5 μm.[14,17,51] Although nodular defects are believed to originate from particulates deposited onto the surface during or before film growth,[52] more work is currently needed to better understand mechanisms of nodule nucleation and growth in B_4C.

6. Mechanical properties

Figure 2(d) shows dependencies of E and H on T_s. A significant increase in both E and H occurs when T_s is increased from 100 to 180 °C. For $T_s > 180$ °C, E increases by $\sim 10\%$ from $\sim$ 300 to 325 GPa, while H remains in the range of $25 - 32$ GPa, following a similar increasing trend to that of E. This trend is generally consistent with the T_s dependence of film density [Fig. 2(b)]. Values of E and H from Fig. 2(d) are comparable with those reported by Kulikovsky et al.[21] for sputter-deposited amorphous B_4C, which exhibited a slight increase in E from $\sim$ 320 to $\sim$ 350 GPa and H from 29 to 33 GPa when T_{holder} was increased from 500 to 700 °C. It is also in agreement with observations of a negligible change in film micro-hardness on increasing T_{holder} from 100 to 300 °C for B_4C films deposited by DCMS onto electrically grounded substrates reported by Knotek et al.[3]

7. Optical properties

In spectroscopic ellipsometry measurements, we have observed a tilting of the interference oscillations for both Ψ and Δ as function of wavelength. This suggests the existence of anisotropy within the films. Hence, we have used a uniaxial anisotropic model, with different optical properties across the film thickness (the extraordinary refractive index, n_z) and in the film plane (the ordinary index, $n_x = n_y$). Such an anisotropic model has given a

slightly better fit to data than an isotropic layer model. Error bars were computed by fitting optical constants for layers whose average thickness was varied by 2.5% from the average value measured. From this analysis, we have found that n_x, n_z, and the extinction coefficient k at 632.8 nm remain constant at 3.2 ± 0.2, 3.4 ± 0.6, and 0.20 ± 0.04, respectively, for all the films deposited at different T_s values. This behavior is consistent with the relatively weak dependence of mass density on T_s [Fig. 2(b)].

8. Film homogeneity

Figure 6 shows 2D-GISAXS data from three representative films deposited at T_s of 185, 240, and 510 °C. A comparison of these Figs. 6(a) – 6(c) shows that the scattering intensity scale in the Yoneda region[53] (i.e., the region of low q_x and q_z) increases with increasing T_s from 185 to 240 °C followed by a scattering intensity decrease for 510 °C. While the scattering intensity changes, the shape of scattering patterns is essentially independent of T_s.

In order to extract the degree of heterogeneity as a function of T_s, one of the 2D-GISAXS pattern was fitted with a model[54] featuring monodispersed cylinders, oriented perpendicular to the film plane and packed in a 2D hexagonal structure, with a Gaussian distribution of the distance between neighboring cylinders. The best fit to the data was obtained for cylinders with an aspect ratio of 4.2, and the mean and standard deviation values of the distance between the centers of adjacent cylinders of 2.9 nm and 2.4 nm, respectively. Fitting of 1D line cuts of 2D-GISAXS patterns showed that the scattering scaling factor (φ) was the model parameter that exhibited a dependence on T_s. It is plotted in Fig. 6(d). Because the size of these heterogenities does not change appreciably with temperature, the parameter φ is proportional to the concentration of the scattering centers (cylinders) and the square of the difference in the electron density in the cylinders and the matrix.

Figure 6(d) shows that φ slightly increases with T_s, reaches a maximum at 240 °C, followed by a monotonic decrease for higher T_s values. The initial increase in φ with increasing T_s for $T_s \lesssim 240$ °C indicates that, in the columnar growth regime, a decrease in residual stress and an increase in E and H are accompanied by an increase in anisotropic heterogeneity. This observation could be related to an increase in the stoichiometric imbalance during columnar growth due to different mobilities of B and C adatoms, as suggested based on transmission electron microscopy measurements in our recent study of the oblique angle deposition of B_4C films.[18] The decrease in φ with increasing T_s at high temperatures could be attributed to a decrease in porosity and a corresponding increase in the mass density [Fig. 2(b)].

IV. CONCLUSIONS

In summary, we have studied the effect of substrate temperature in the range of $100 - 510$ °C on the structural, mechanical, and optical properties of B_4C thin films deposited by direct current magnetron sputtering in the low-residual-stress regime. All deposited films are amorphous, stoichiometric, and with low impurity content. The mass density, surface roughness, and mechanical properties of the films are weakly and monotonically dependent on T_s. In contrast, residual stress and film density homogeneity exhibit a non-monotonic behavior on T_s, with the minimum compressive stress and the maximum degree of inhomogeneity for a T_s of 240 °C. These results indicate that, at least for the deposition conditions studied here, if the lowest intrinsic residual stress is desired, an intermediate range of T_s of $185 - 250$ °C should be chosen, while, for largest mechanical properties, highest density, and best density uniformity, higher substrate temperatures are preferred. Higher substrate temperatures are particularly attractive in cases when the total residual stress can be minimized by the choice of a substrate with a specific CTE. The overall weak dependence of all the major properties on T_s is attractive for the development of robust processes for the deposition onto non-planar substrates for which accurate control of T_s is often not feasible or economical.

V. ACKNOWLEDGMENTS

This work was performed under the auspices of the U.S. DOE by LLNL under Contract DE-AC52-07NA27344 and by General Atomics under Contract 89233119CNA000063 and was supported by the LLNL-LDRD program under Project No. 20-ERD-029.

[1] F. Thevenot, Boron carbide – A comprehensive review, J. Europ. Ceram. Soc. **6**, 205 (1990).

[2] E. Eichen, J. D. Flasck, Ovonic Synthetic Materials Co Inc, 1987. Disordered coating. U.S. Patent 4,716,083.

[3] O. Knotek, E. Lugscheider, and C. W. Siry, Superhard PVD coatings in the B-C-N triangle, Int. J. Refract. Met. H. **17**, 157–162 (1999).

[4] G. L. Doll, The Timken Company, 2003. Bearing with amorphous boron carbide coating. U.S. Patent 6,517,249 B1.

[5] R. F. Boland, C. A. Hultman, W. E. Vreeland, P. S. Williams, Warner-Lambert Company, 1992. Shaving razors. U.S. Patent 5,088,202.

[6] D. L. Windt, Reduction of stress and roughness by reactive sputtering in W/B_4C X-ray multilayer films, Proc. SPIE

6688, R6880–R6880 (2007).

[7] R. Soufli, A. L. Aquila, F. Salmassi, M. Fernández-Perea, and E. M. Gullikson, Optical constants of magnetron-sputtered boron carbide thin films from photoabsorption data in the range 30 to 700 eV, Appl. Optics **47**, 4633–4639 (2008).

[8] J. L. Wu, R. Z. Qi, Q. S. Huang, Y. F. Feng, Z. S. Wang, and Z. H. Xin, Stress, roughness, and reflectivity properties of sputter-deposited B_4C coatings for x-ray mirrors, Chin. Phys. Lett. **36**, 120701 (2019).

[9] C. Höglund, J. Birch, K. Andersen, T. Bigault, J. C. Buffet, J. Correa, P. van Esch, B. Guerard, R. Hall-Wilton, J. Jensen, A. Khaplanov, F. Piscitelli, C. Vettier, W. Vollenberg, and L. Hultman, B_4C thin films for neutron detection, J. Appl. Phys. **111**, 104908 (2012).

[10] Z. Zhang, Y. Liang, W. Li, Z. Wang, and H. Chen, Stress evolution in B_4C and Cr mono-layer and B_4C/Cr multilayer with variable layer thickness for neutron detectors, Thin Solid Films **531**, 302–305 (2013).

[11] O. I. Buzhinskij, and Y. M. Semenets, Thick boron carbide coatings for protection of tokamak first wall and divertor, Fusion Eng. Des. **45**, 343–360 (1999).

[12] H. Shih, N. Han, S. S. Y. Mak, G. Z. Yin, Applied Materials Inc, 2000. Boron carbide parts and coatings in a plasma reactor. U.S. Patent 6,120,640.

[13] T. R. Dittrich, S. W. Haan, S. Pollaine, A. K. Burnham, and G. L. Strobel, NIF capsule design update, Fusion Sci. Tech. **31**, 402 (1997).

[14] A. K. Burnham, C. S. Alford, D. M. Makowiecki, T. R. Dittrich, R. J. Wallace, E. C. Honea, and C. M. King, Evaluation of B_4C as an Ablator Material for NIF Capsules, Fusion Sci. Tech. **31**, 456 (1997).

[15] A. S. Moore, S. Prisbrey, K. L. Baker, P. M. Celliers, J. Fry, T. R. Dittrich, K J. J. Wu, M. L. Kervin, M. E. Schoff, M. Farrell, A. Nikroo, and O. A. Hurricane, A simulation-based and analytic analysis of the off-Hugoniot response of alternative inertial confinement fusion ablator materials, High Energy Density Phys. **20**, 23 (2016).

[16] R. Chen, J. Qi, Q. Shi, X. Guo, D. Wu, T. Lu, and Z. Liao, Rapid preparation and uniformity control of B_4C ceramic double-curvature shells: Aim to advance its applications as ICF capsules, J. Alloys Compd. **762**, 67 (2018).

[17] A. M. Engwall, L. B. Bayu Aji, S. Shin, P. B. Mirkarimi, J. H. Bae, and S. O. Kucheyev, Sputter-deposited low-stress boron carbide films, J. Appl. Phys. **128**, 175301 (2020).

[18] S. J. Shin, L. B. Bayu Aji, J. H. Bae, A. M. Engwall, M. H. Nielsen, J. A. Hammons, X. B. Zuo, B. Lee, X. Lepro Chavez, P. B. Mirkarimi, and S. O. Kucheyev, Oblique angle deposition of boron carbide films. J. Appl. Phys. (accepted).

[19] T. Hu, L. Steihl, W. Rafaniello, T. Fawcett, D. D. Hawn, J. G. Mashall, S. J. Rozeveld, C. L. Putzig, J. H. Blackson, and W. Cermignani, Structures and properties of disordered boron carbide coatings generated by magnetron sputtering, Thin Solid Films **332**, 80–86 (1998).

[20] M. L. Wu, J. D. Kiely, T. Klemmer, Y. T. Hsia, K. Howard, Process property relationship of boron carbide thin films by magnetron sputtering, Thin Solid Films **449**, 120 (2004).

[21] V. Kulikovsky, V. Vorlicek, P. Bohac, R. Ctvrtlik, M. Stranyanek, A. Dejneka, and L. Jastrabik, Mechanical properties and structure of amorphous and crystalline B_4C films, Diamond & Rel. Mat. **18**, 27–33 (2009).

[22] S. Schmidt, C. Höglund, J. Jensen, L. Hultman, J. Birch, and R. Hall-Wilton, Low-temperature growth of boron carbide coatings by direct current magnetron sputtering and high-power impulse magnetron sputtering, J. Mater. Sci. **51**, 10418 (2016).

[23] L. Jacobsohn, R. Averitt, and M. Nastasi, The role of trapped Ar atoms in the mechanical properties of boron carbide films deposited by dc-magnetron sputtering, J. Vac. Sci. Technol. A **21**, 1639–1643 (2003).

[24] M. A. McKernan, Magnetron sputter deposition of boron and boron carbide, Surf. Coat. Technol. **49**, 411–415 (1991); Erratum Surf. Coat. Technol. **53**, 199 (1992).

[25] J.A.Thornton, High-rate thick-film growth, Annu. Rev. Mater. Sci. **7**, 239 (1977).

[26] A.G. Dirks and H.J. Leamy, Columnar microstructure in vapor-deposited thin films, Thin Solid Films **47**, 219 (1977).

[27] R. Messier, A. P. Giri, and R. A. Roy, Revised structure zone model for thin film physical structure, J. Vac. Sci. Technol. A **2**, 500 (1984).

[28] L. Abelmann and C. Lodder, Oblique evaporation and surface diffusion, Thin Solid Films **305**, 1 (1997).

[29] R. Bao, and D. B. Chrisey, Short range order structure of amorphous B_4C boron carbide thin films, J. Mater. Sci. **46**, 3952–3959 (2011).

[30] C. Chiang, H. Holleck, and O. Meyer, Properties of RF sputtered B_4C thin films, Nucl. Instrum. Methods Phys. Res. B **91**, 692–695 (1994).

[31] Z. Han, G. Li, J. Tian, and M. Gu, Microstructure and mechanical properties of boron carbide thin films, Mater. Lett. **57**, 899–903 (2002).

[32] E. Pascual, E. Martínez, J. Esteve, A. Lousa, Boron carbide thin films deposited by tuned-substrate RF magnetron sputtering. Diam. Relat. Mater. **8**, 402 (1999).

[33] S. D. Nehate and K. B. Sundaram, Investigations of electrical and optical properties of hydrogen doped boron carbide thin films, ECS Transactions **85**, 1607 (2018).

[34] T. S. Kim, J. H. Yeo, K. B. Nam, M. J. Kim, and J. B. Yoo, Boron carbide coating to improve the chemical stability of nm-thick graphite, Thin Solid Films **704**, 138002 (2020).

[35] F. Kaminaga, S. Sato, and Y. Okamoto, Evaluation of gap heat transfer between boron carbide pellet and cladding in control rod of FBR, J. Nucl. Sci. Technol. **29**, 121 (1992).

[36] L. S. Doolittle, Algorithms for the rapid simulation of rutherford backscattering spectra, Nucl. Instrum. Methods Phys. Res. B **9**, 344–351 (1985).

[37] G. C. Janssen, M. Abdalla, F. Van Keulen, B. Pujada, and B. Van Venrooy, Celebrating the 100th anniversary of the Stoney equation for film stress: Developments from polycrystalline steel strips to single crystal silicon wafers, Thin Solid Films **517**, 1858–1867 (2009).

[38] L. B. Freund and S. Suresh, Thin Film Materials: Stress, Defect Formation and Surface Evolution, Cambridge University Press: Cambridge, 2004. pp 86-101.

[39] W. C. Oliver and G. M. Pharr, An improved technique for determining hardness and elastic modulus using load and displacement sensing indentation experiments, J. Mater. Res. **7**, 1564 (1992).

[40] S. O. Kucheyev, A. V. Hamza, J. H. Satcher Jr, and M. A. Worsley, Depth-sensing indentation of low-density brittle nanoporous solids, Acta Mater. **57**, 3472 (2009).

[41] D. Babonneau, *FitGISAXS*: software package for modelling and analysis of GISAXS data using IGOR Pro, J. Appl. Crystallogr. **43** 929 (2010).

[42] J. T. Gudmundsson and A. Hecimovic, Foundations of DC plasma sources, Plasma Sources Sci. Technol. **26** 123001 (2017).
[43] H. Watanabe, N. Yamada, and M. Okaji, Linear thermal expansion coefficient of silicon from 293 to 1000 K, Int. J. Thermophys. **25** 221–236 (2004).
[44] G. V. Tsagareishvili, T. G. Nakashidze, J. Sh. Jobava, G. P. Lomidze, D. E. Khulelidze, D. Sh. Tsagareishvili, and O. A. Tsagareishvili, Thermal expansion of boron and boron carbide, J. Less Common Met. **117**, 159 (1986).
[45] W. M. Haynes, D. R. Lide, and T. J. Bruno. CRC Handbook of Chemistry and Physics: A Ready-reference Book of Chemical and Physical Data. CRC Press (2016).
[46] H. Windischmann, Intrinsic stress in sputter-deposited thin films, Crit. Rev. Solid State Mater. **17**, 547 (1992).
[47] S. Lichter and J. Chen, Model for columnar microstructure of thin solid films, Phys. Rev. Lett. **56**, 1396 (1986).
[48] A. Mazor, D. J. Srolovitz, P. S. Hagan, and and B. G. Bukiet, Columnar growth in thin films, Phys. Rev. Lett. **60**, 424 (1988); Erratum Phys. Rev. Lett. **60**, 1455 (1988).
[49] R. P. U. Karunasiri, R. Bruinsma, and J. Rudnick, Thin-film growth and the shadow instability, Phys. Rev. Lett. **62**, 788 (1989).
[50] G. S. Bales, R. Bruinsma, E. A. Eklund, R. P. U. Karunasiri, J. Rudnick, and A. Zangwill, Growth and erosion of thin solid films, Science **249**, 264–268 (1990).
[51] C. Mattsson, G. Randall, H. Xu, J. Knipping, D. Wall, B. Blue, and A. Nikroo, Boron carbide materials for inertial confinement fusion, Poster presentation at 55th Annual Meeting of the APS Division of Plasma Physics, Denver, Colorado, November 11–15, (2013).
[52] P. Panjan, A. Drnovsek, P. Gselman, M. Cekada, and M. Panjan, Review of growth defects in thin films prepared by PVD techniques, Coatings **10**, 447 (2020).
[53] Y. Yoneda, Anomalous surface reflection of x-rays, Phys. Rev. **131**, 2010 (1963).
[54] G. Renaud, R. Lazzari, and F. Leroy, Probing surface and interface morphology with Grazing Incidence Small Angle X-Ray Scattering, Surf. Sci. Rep. **64**, 255 (2009).
[55] L. G. Jacobsohn, M. Nastasi, Sputter-deposited boron carbide films: Structural and mechanical characterization, Surf. Coat. Technol. **200**, 1472 (2005).